Effect of the Functionalization Process on the Colloidal, Magnetic Resonance Imaging, and Bioelimination Properties of Mono- or Bisphosphonate-Anchored Dendronized Iron Oxide Nanoparticles

Aurélie Walter, Antonio Garofalo, Pauline Bonazza, Florent Meyer, Hervé Martinez, Solenne Fleutot, Claire Billotey, Jacqueline Taleb, Delphine Felder-Flesch, Sylvie Begin-Colin

A GENUINELY MULTIDISCIPLINARY JOURNAL

CHEMPLUSCHEM

CENTERING ON CHEMISTRY

Accepted Article

Title: Effect of the functionalization process on colloidal, MRI and bioelimination properties of mono or bisphosphonate-anchored dendronized iron oxide nanoparticles

Authors: Sylvie Begin-Colin, Aurelie Walter, Antonio Garofalo, Pauline Bonazza, Florent Meyer, Hervé Martinez, Solenne Fleutot, Claire Billotey, Jacqueline Taleb, and Delphine Felder

To be cited as: *ChemPlusChem* 10.1002/cplu.201700049

Link to VoR: http://dx.doi.org/10.1002/cplu.201700049

A Journal of

ChemPubSoc Europe

WILEY-VCH

www.chempluschem.org

10.1002/cplu.201700049

WILEY-VCH

Effect of the functionalization process on colloidal, MRI and bioelimination properties of mono or bisphosphonate-anchored dendronized iron oxide nanoparticles

A. Walter[a], A. Garofalo[a], P. Bonazza, [b] F. Meyer[c], H. Martinez[d], S. Fleutot[a], C. Billotey[b],J. Taleb, [b] D. Felder-Flesch* [a], S. Begin-Colin* [a]

Abstract: The functionalization process of iron oxide nanoparticles (NPs) is a major step and has to ensure a small particle size distribution (below 100 nm) and to preserve good magnetic properties suitable for in vivo applications. Two functionalization processes are here compared to coat iron oxide NPs, synthesized by thermal decomposition, with dendron molecules bearing either a mono- or a bis-phosphonate anchoring group: the direct ligand exchange or the simultaneaous ligand exchange and phase transfer process. This last process led to larger size distribution than the former. The phosphonate group is confirmed to be a strong anchoring agent from XPS and IR characterizations whatever the grafting process and the number of phosphonate groups and to preserve NPs magnetic properties. All dendronized NPs display good in vitro MRI properties and those obtained by direct exchange showed no cell internalization, an efficient in vivo MRI contrast enhancement and an elimination by both urinary and hepato-biliary ways.

Introduction

Iron oxide nanoparticles (NPs) are extensively studied for their high potential in biomedical applications mainly as contrast agent for MRI, heating mediator for hyperthermia, or nanoplateforms for drug delivery. [1-8] Besides the magnetic properties of the iron oxide core which are very important for MRI and magnetic hyperthermia applications[2], the design and control of the NPs coating is also of upmost importance as it will be in contact with the biological media and determine the biological outcome of the final hybrid object. Indeed surface coating of the NPs must promote biocompatibility and reduce nonspecific biological interactions (i.e. uptake by the reticulo endothelial system or opsonisation) while maintaining an overall compact size mandatory for in vivo injection. Specific coating and mean particle size in physiological media smaller than 100 nm are required for long term stability over a broad pH range as well as for optimal biodistribution of NPs in the presence of high concentration of electrolyte and in biological (protein rich) media. Indeed long blood-circulation time would maximize the possibility to reach target tissue: suspensions of particles with average hydrodynamic sizes of 10–100 nm are optimal for *in vivo* delivery, as smaller ones (<10 nm) are rapidly removed by renal clearance while bigger ones (>200 nm) are quickly sequestered by the reticuloendothelial system. For targeted drug delivery or MRI, the NPs coating must promote the circulation and a long lifetime in the blood stream (e.g. good biodistribution). NPs coating should also provide functional moieties such as targeting ligands or fluorescent molecules allowing the design of multifunctional hybrid NPs.

The main NPs coatings can be classified in inorganic and organic coating materials. Silica and gold are the mainly used inorganic coatings but their further coating by biocompatible molecules is needed for biomedical applications. Different classes of organic coatings can be distinguished: small ligands/molecules (adenosine triphosphate, bifunctional and discrete PEG chains including silane, dendrons,), polymers or lipids. Natural and synthetic polymers such as dextran, PEG, polyvinyl alcohol, alginate, chitosan have been often used as polymeric stabilizers.[3,4,5,6,7,8] For *in vivo* applications which require functionalized NPs with a good biodistribution,[9] small molecules are more and more developed among which dendron molecules[10,11,12,13,14] which were shown to provide small mean hydrodynamic size compatible with long time blood circulation. Dendrimers and dendron discrete building blocks are indeed promising as the diversity of functionalization brought by the arborescent structure simultaneously solves the problems of biocompatibility, low toxicity, large in vivo stability and specificity.[11,12,13,14] Moreover, in addition to a controlled multifunctionalization, dendrimers and dendron units allow a versatility of size (according to generation) and of physicochemical properties (hydrophilic, lipophilic) which can be tuned. The resulting effects on stability (dendrimer effect), pharmacokinetics and biodistribution can then clearly be identified.

[a] A. Walter, A. Garofalo, S. Fleutot, ,D. Felder-Flesch*, S. Begin-Colin*
Institut de Physique et Chimie des Matériaux de Strasbourg (IPCMS), UMR 7504, CNRS, Université de Strasbourg, 23, rue du Loess, BP 43, 67034 Strasbourg Cedex 2 (France). Fax: sylvie.begin@unistra.fr, delphine.felder@ipcms.unistra.fr
[b] P. Bonazza, J. Taleb, C. Billotey
Université de Lyon, Université Jean Monnet, Equipe Mixte de Recherche 3738 « Ciblage Thérapeutique en Oncologie », France [
[c] F. Meyer
INSERM 1121, Faculté de Chirurgie Dentaire, Université de Strasbourg, 11, rue Humann, 67000 Strasbourg Cedex
[d] H. Martinez
IPREM – UMR CNRS 5254, Université de Pau et des Pays de l'Adour, Hélioparc Pau-Pyrénées, 2 Av du Président Angot, 64053 Pau Cedex 9, France

Supporting information for this article is given via a link at the end of the document.

Another key parameter in the design of coating is its anchoring at the NPs surface which has to be strong to avoid desorption and replacement by proteins after *in vivo* injection. To ensure a strong anchoring of molecules at the NPs surface, various anchoring groups including carboxylates[15,16,17,18,19], catechol[20,21], phosphonate[9, 22, 23, 24, 25, 26, 27] based ligands have been developped. [28] Among them, the phosphonate moiety was introduced as an effective anchoring agent because of the high ability of $-PO(OH)_2$ groups to complex metal ions and to form complexes which are stable even at elevated temperature.[26, 29, 30, 31] A significantly higher grafting rate and stronger binding than those obtained with carboxylate anchors have been evidenced.[22,23, 32] Previous works on such dendronized NPs demonstrated a good colloidal stability in water and osmolar media and very high enhancement contrast ratio (EHC) values at high magnetic field.[25,24] The coupling with a fluorophore made these nanoprobes effective for multimodal imaging.[33]

The final mean hydrodynamic size of functionnalized NPs depends strongly on the grafting process. The NPs may be synthesized in the presence of biocompatible ligands but more and more often the functionalization step occurs after the NPs synthesis step. Two major approaches are then reported and depend on the NPs synthetic method. When naked NPs are obtained as with coprecipitation or polyol approaches, the molecules are introduced in the NPs water suspension at suitable pH depending on anchoring and functional groups at their surface[27,33] and direct grafting occurs. When NPs are *in situ* coated during their synthesis step as with the more and more used decomposition methods of metal precursor in organic solvants in controlled conditions, direct ligand exchange may be realized by just introducing the molecules in the organic solvant if the biological molecules are soluble in the organic solvant. Then the coated NPs are transfered in water. Otherwise a ligand exchange and phase transfer process may be realized and consists in putting into contact a water suspension of molecules with the NPs suspension in a hydrophobic solvant. Both processes are based on the higher affinity of the new ligand anchoring group towards the iron oxide surface compared to the original one (often oleic acid or oleylamine).

With NPs synthesized by thermal decomposition, both processes are developped but some problems are evidenced : some oleic acid molecules remains at the NPs surface needing two exchange steps to push the exchange rate and some hydrophobic solvants are difficult to remove without a freeze drying step. Recently, Felder et al demonstrated that biphosphonated dendrons allow decreasing strongly the remaining oleic acid ligands after only one direct exchange step, showing that bis-anchoring molecules are promising not only to ensure a strong anchoring of molecules at the surface of NPs but also to lower unspecific cellular uptake.[34]

In that context, this paper aims at investigating the grafting either by direct ligand exchange or by a ligand exchange and phase transfert process, of dendrons molecule bearing either one (dendron D2) or two (dendron D2-2P) phosphonate anchoring groups (Figure 1). Compared to our previously reported dendritic coating (ANACOOH)[24,25,27,33] a linker between the dendritic hydrophilic part and the phosphonic acid focal point has been introduced to facilitate the dendron anchoring at the NP surface, to increase the grafting rate and make easier the synthesis of the dendron molecule. The anchoring strength, the colloidal stability, the grafting rate and the MRI properties will be discussed by considering the effect of the number of anchoring group and of the grafting way.

Results and Discussion

Validation of the grafting of dendron at the surface of NPs

Iron oxide NPs with an average of 10 nm ± 10% were synthesized by thermal decomposition of an iron stearate complex in the presence of oleic acid (OA) as surfactant in a high boiling point solvent (Figure S1). X-ray diffraction showed that they display the typical iron oxide spinel structure as already reported.[35,36]. The NPs synthesized by thermal decomposition are *in situ* coated by oleic acid and formed very stable suspension in organic solvent (Figure S1b). The average hydrodynamic diameter of 13 nm determined by granulometric measurements is slightly larger than the mean diameter deduced from TEM micrographs (Figure S1a) due to the oleic acid surface coating.

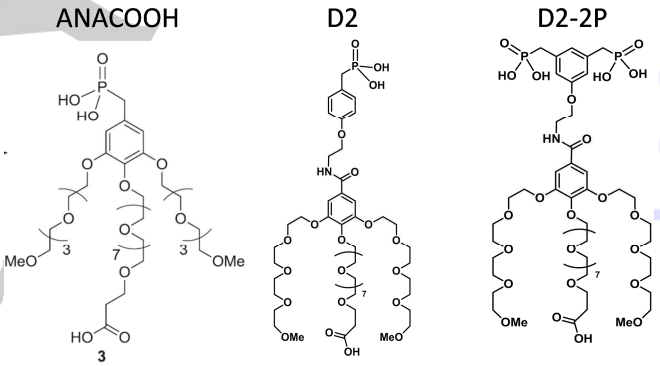

Figure 1 : Scheme of the earlier used dendron ANACOOH and of dendron molecules used to functionalize the NPs

Two dendron molecules, soluble in both water or THF, were grafted on the surface of the NPs using two different grafting methods. The dendron molecules architecture are presented in Figure 1. These highly water soluble and biocompatible functional dendrons[27,33] possess (i) one (D2) or two (D2-2P) phosphonic acids as anchoring groups providing a strong binding to NPs, (ii) PEG chains providing biocompatibility and suspension stability and (iii) functional ending groups allowing further coupling of fluorophores or biomolecules of interest. Furthermore, earlier studies have demonstrated that when the dendron bears a functional carboxylate peripherical end group, a better colloidal stability in physiological media is observed as well as a better *in vivo* bioditribution.[27,33]

The grafting of dendrons D2 and D2-2P either by a direct ligand exchange (DE) process or by a phase transfer (PT) process has been compared. In the first method, the NPs and the new ligand

were mixed together and magnetically stirred for at least 24h in an organic solvent such as THF and then transfered in water. While in the case of the second method, the NPs and the molecules were in separate phases: the NPs were dispersed in an organic hydrophobic solvent such as hexane and the molecule was diluted in an aqueous solution at a given pH.[27,33] Under magnetic stirring, the two phases were mixed and slowly the NPs grafted with the dendron transferred in the water phase.[27] In the following, NP@D2-DE refers to NPs functionalized through the direct exchange process (DE) and NP@D2-PT refers to NPs functionalized by the phase transfer (PT) ligand exchange process.

For both functionnalization methods, the amount of oleic acid was shown to be very important to ensure a high ligand exchange rate: it has to be as low as possible to push the exchange rate as high as possible. Furthermore in the case of the PT process, a low oleic acid amount was necessary to avoid the formation of oleic acid based micelles at the water/organic solvent interface which otherwise pertubates strongly the ligand exchange process. Therefore, the washing of the as-synthesized NPs coated with OA has been investigated by trying to remove the maximum of OA while simultaneously preserving the colloidal stability. The OA removal was followed by IR spectroscopy and we observed that an optimum exchange is obtained when the IR intensities of the ν_{CH2} bands of OA around 2800 cm^{-1} and of the Fe-O band around 600 cm^{-1} are similar in intensity (Figure S2). TGA experiments highlighted that this washing process leads to roughly an OA monolayer at the surface of NPs.[37]

The grafting of the dendron molecules on the surface of the NPs is confirmed by infrared spectroscopy where the characteristic bands of dendrons are indexed in IR spectra of purified dendronized NPs. The IR spectra of D2 and D2-2P are very similar (Figure S3a), as their architectures are, except at the focal point. The symmetric and asymmetric vibration bands of the benzyl C-H groups are observed in the spectra. The C=O band is associated to the carboxylic acid group localized at the dendrons periphery. The numerous bands between 1300 and 1110 cm^{-1} are attributed to the N-H and N-CO groups. The C-H bands present on the PEG chains are also identified. The intense and large band localized at 1110 cm^{-1} is attributed to the C-O-C bands from the PEG chains and the C-C-C band from the benzyl group. The IR spectra of NPs functionalized with D2 and D2-2P being similar (Figure S3), only the IR spectra of NP functionalized with D2 either by direct exchange (NP@D2-DE) or by phase transfer process (NP@D2-PT) are detailed in Figure 2.

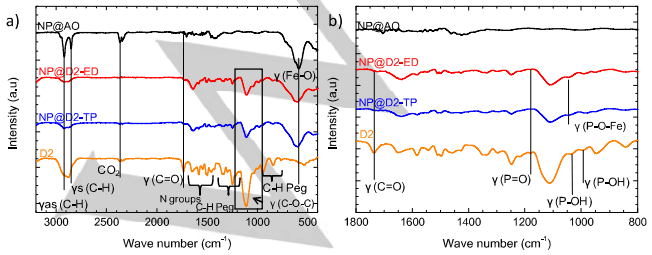

Figure 2 : IR spectra a) of NPs before and after functionalization with D2 by DE or PT b) IR spectra in the phosphonate bands zone

After functionalization, the characteristic bands of dendrons D2 are identified on the spectra of the dendronized NPs (Figure 2a) and the phosphonate bands in the range 900-1200 cm^{-1} evolved confirming the grafting through this group (Figure 2b). The precise localization of P-OH and P=O bands of dendron is difficult to assign as they display several IR bands with some overlapping. A previous fine IR characterization of dendrons at different synthetic steps[33] allowed identifying the P=O band around 1180 cm^{-1}, and the P-OH bands at 1037 and 994 cm^{-1}. An additional band is observed at 1737 cm^{-1} related to the C=O band of the carboxylic acid function but this band is strongly reduced after functionalization due to the protonation of this group after water transfer. For functionalized NPs, the intensity of the P=O band strongly decreased after the grafting step, and the P-OH bands disappeared while new bands appeared due to a modification of the electronic density around the atoms with the formation of the Fe-O-P bond (1045 cm^{-1}).[25] These observations confirm the grafting of the D2 molecule on the NPs surface through the $P(O)(OH)_2$ group according to the two functionalization methods. The same observations can be made for the NPs functionalized with the molecule D2-2P.

The grafting rate was determined by elemental analysis of iron and phosphorus in each sample, and by considering that the surface covered by D2 and D2-2P is equal to 0.75 nm^2, a value deduced from the area of a PEG chain which is about 0.25 nm^2. The theoretical amount of grafted molecules is thus ~1.4 molecules /nm^2 for both D2 and D2-2P. The grafting rate was determined to be 1.6 ±0.3 molecule/nm^2 and 1.7 ±0.3 molecule/nm^2 for NP@D2 and NP@D2-2P respectively after a direct ligand exchange. The grafting is slightly lower after phase transfert and ligand exchange: ~ 1.4 ±0.3 molecule/nm^2. The comparison of experimental and theoretical grafting rate suggests a good coverage of the NPs surface by dendrons D2 and D2-2P whatever the grafting process or the number of anchoring groups.

Additional XPS measurements were performed on dendronized NPs to evaluate the effect of the grafting method on the strength of the phosphonate anchoring. The O1s core peaks of NP@OA[27] and NP@D2 or NP@D2-2P (Figure S4) displayed two and three components respectively. For NP@OA, previous results reported a peak located at 530.4 eV corresponding to Fe-O bonds.[27] The other component located at 532.3 eV is associated to -COO- bonds due to their oleic acid coating. After the grafting of the phosphonate-based molecules, additional peaks, beside the one due to Fe-O bonds at around 530.5 eV, were located at binding energies of around 531.1 eV and 532.9 eV (Figure S4). The first one corresponded to the contributions of P-O bonds (P=O, P–OH, Fe–O–P) in agreement with the bibliographic data that reported the binding energies of M–O–P (M = metal), P=O and P-OH in the range 531.1 – 532.2 eV.[38] However one may notice that this peak is slightly shifted depending on the grafting way: 531 eV for the ligand exchange by phase transfer and 531.3 eV for that by direct exchange. This

suggests that the chemical environment of phosphorus atoms is different depending on the functionalization method.

The P2p spectrum (Figure 3) of phosphonate dendron molecules exhibited two components at ~133.9 and 134.8 eV, corresponding to $P2p_{3/2}$ and $P2p_{1/2}$ respectively.[27] The 2p $^3/_2$-$^1/_2$ peaks presented a low bonding energy difference between both $^3/_2$ and ½ components due to a spin orbit coupling of about 0.9 eV. When the dendrons were grafted on the NPs, a broadening and a shift of the peaks towards lower binding energies was observed. Such shifting has already been observed in the case of the grafting of the other type of dendron (ANACOOH) at the surface of NPs synthesized by co-precipitation and thermal decomposition.[27] This shift is attributed to the formation of P-O-Fe bonds. The chemical shift (1eV) is observed to be smaller with NPs functionalized by direct exchange than with NPs functionalized by phase transfer (1.3 eV). The both observed chemical shifts indicate that the chemical surrounding around the phosphorus atoms is different and that a strong anchoring through the phosphonate group occurred for both grafting methods. However the surface anchoring appears stronger in the case of the ligand exchange by phase transfer. This may be explained by enhanced electrostatic interactions that occur, during the phase transfer method, between the dendron and iron oxide NPs which should favor stronger anchoring conditions. Indeed, the dendron molecules are in water at pH 3.5 and thus partially deprotonated (negatively charged) and hydroxide groups at the surface of the NPs are protonated leading to a positively charged NPs surface. In previous studies, we demonstrated that phosphatation of iron oxide NPs was favored by the fact that deprotonated phosphonates (negatively charged) interacted with both positively charged groups and hydroxyl sites at the surface of NPs.[22,23] Thus the electrostatic interactions between phosphonate groups and the positively charged NPs surface should favor a stronger anchoring of phosphonates at the iron oxide surface by comparison with the direct ligand exchange which occurs in organic solvent (very low amount of water) and for which the anchoring takes place mainly by interaction of dendron phosphonate group and OH groups at the NPs surface. Another important result deduced from this XPS study is that whatever the number of phosphonate anchoring group, the results are similar confirming a strong anchoring in both cases.

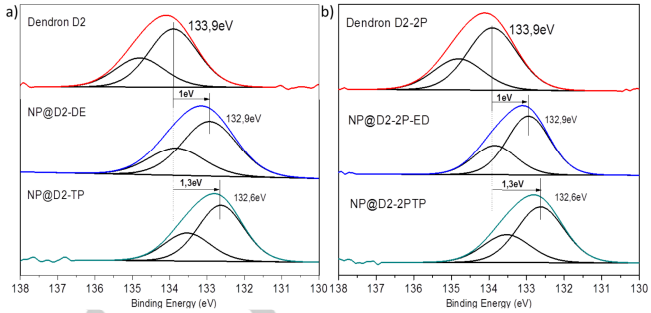

Figure 3 : a) P2p XPS spectra of D2, NP@D2-ED, NP@D2-PT b) P2p spectra of D2-2P, NP@D2-2P-ED, NP@D2-2P-PT

Colloidal stability of dendronized NPs and MRI properties

The particle size distributions of NP@D2 and NP@D2-2P suspensions were determined by Dynamic Light scattering (DLS). Depending on the grafting strategy, the average hydrodynamic diameter and size distribution were strongly different (Figure 4). Indeed, after the DE process, a monomodal size distribution with an average diameter close to 20 nm is obtained, while, after the PT process, the suspensions displayed a monomodal size distribution centered at around 110 nm for NP@D2-PT and a bimodal size distribution (centered at 180 and 450 nm) for NP@D2-2P-PT. These PT suspensions quickly precipitated while the NPs functionalized by DE were stable in suspension over a long time scale.

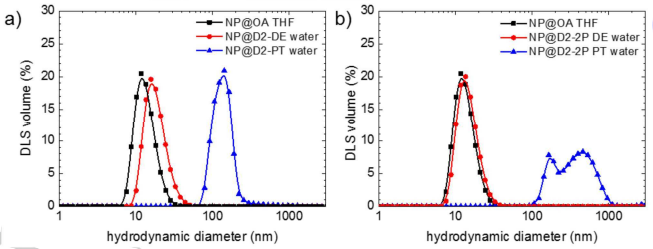

Figure 4 : Particle size distribution of a) NP before and after grafting of D2 by DE and PT b) NP before and after grafting of D2-2P by DE and PT

These experiments were reproduced several times and the same results were obtained (Table S1). The phase transfer process (PT) leads here to dendronized NPs suspensions with larger mean hydrodynamic diameter and less stable suspensions than the direct ligand exchange process. In our earlier studies with other dendron architectures, an aggregation of NPs has always been observed[27] and only low concentration conditions succeeded in obtaining good size distribution with PAMAM based dendrons.[39] Indeed, the process of ligand exchange with phase transfer failed to maintain the initial size distribution of NP@OA : aggregates formed during the phase transfer step due to the fact that close to the solvant interface, NPs instabilities exist: NPs are partially coated with oleic acid (as oleic acid molecules desorb to move towards the water/organic sovant interface) and are not completely coated with hydrophilic dendrons which favors their aggregation through Van der Waals interactions (Figure S5). One may notice that the agregation observed with these dendrons is larger than that noticed in earlier studies with ANACOOH and may be related to the dendron architecture which display an added part/linker (Figure 1). This result suggests thus that the molecule nature/architecture may affect the ligand exchange process.

Thus the ligand exchange with phase transfer strategy leads to a stronger anchoring of the dendron molecule at the surface of the NPs but to less stable NPs suspension with a hydrodynamic size higher than 100 nm. For biomedical applications, the size and size distribution are important parameters. The size should be less than 100 nm. Thus, the direct grafting process was chosen to prepare NPs suspension with the different dendrons (D2 and D2-2P) in order to study their magnetic and relaxivity properties.

Structural and magnetic characterizations

XRD patterns recorded before and after functionalization with dendron molecules showed that a slight oxydation occurs after the grafting step. As shown in Figure S6, the characteristic diffraction peaks observed in NP@OA and NP@D2 XRD patterns are indexed with the spinel iron oxide structure. However Magnetite is an inverse spinel: $Fe^{3+}_A[Fe^{2+}Fe^{3+}]_BO_4^{2-}$. However at the nanoscale, the Fe^{2+} ions in octahedral (B = *Oh*) sites are very sensitive to oxidation. The oxidation of Fe^{2+} into Fe^{3+} is accompanied by vacancy formation (□) giving the general formula $Fe^{3+}_A[Fe^{2.5+}_{2-6\delta}Fe^{3+}_{5\delta}\square_\delta]_BO_4^{2-}$. The complete oxidation corresponds to δ = 1/3 and leads to maghemite γ-Fe_2O_3. The XRD patterns of magnetite and maghemite are very similar and the lattice parameter are very close which makes it difficult to discriminate between magnetite and maghemite.[22,23,32,35] The lattice parameters before and after DE dendronisation, determined from the Rietveld refinement are : 8.379 ±0.008 Å and 8.362 ±0.008 Å respectively. Both values are between those of bulk maghemite (8,358 Å) and bulk magnetite (8,396 Å) but, after functionalization, the lattice parameter get closer to the maghemite lattice parameter value. This suggested that, during the grafting, NPs undergo a slight oxidation. Such slight oxidation was already reported in the case of iron oxide ANACOOH dendronization with phosphonate groups.[25] The slight oxidation of the NPs was also confirmed by infrared spectroscopy. Indeed, the fine analysis of the Fe-O band in the IR spectra between 800 and 400 cm^{-1} before and after functionalization highlights the NPs composition evolution after the dendron grafting (Figure S7). The minimum of the Fe-O characteristic band is slightly shifted towards higher values. For NP@OA, the band minimum is localized at 592 cm^{-1} and after functionalization the minimum is displaced at 599 cm^{-1}. Thus after grafting, the NPs composition get closer to maghemite (which minimum is located at 640 cm^{-1}) but stays between magnetite and maghemite. Furthermore, this oxidation is stable in time. Indeed, no further shift of the band minimum could be observed on the IR spectra even 6 month after the grafting step. Thus, the dendronization of the iron oxide NPs through a phosphonate group protects the NPs from oxidation on a long time scale.

As these dendronized NPs are aimed to be used as contrast agent for MRI, their magnetic properties were also investigated before and after the functionalization process. ZFC/FC curves are characteristic of superparamagnetic NPs (Figure S8) and the maximum of the ZFC curves which may be assimilated to the blocking temperature is shifted towards lower temperatures after the dendronization step. This shift is attributed to a decrease of dipolar interactions induced by the dendronization which contributes to increase the interparticle distances.

At 300K no hysteresis loops are observed on magnetization curves for any samples while at 5K the cycles are open in agreement with superparamagnetic behavior at room temperature and of the ferrimagnetic behavior at low temperature (Figure S9). A slight increase of the saturation magnetization Ms at 300K and 5K is observed following the dendron grafting to the surface of the NPs (Table 1). This phenomenon has already been observed in the case of ANACOOH dendronized NPs synthesized by coprecipitation and has been assigned to an increase in the magnetic order in the canted surface layer after the phosphonates grafting to the surface of the NPs.[23,32,40] For NPs dendronized by ligand exchange and phase transfer with dendron ANACOOH, only a conservation of Ms was noticed.[27] The Ms value is thus preserved despite the slight oxidation of NPs. That was attributed earlier to the surface magnetic spin reordering induced by the formation of iron-phosphonate surface complex.[22] The evolution of the spin canting in NP@D2-DE was studied by FC magnetization measurements, e.g. magnetic measurements after cooling down the sample in a field of 2T. Figure S10 compared the FC and ZFC curves of NP@OA and NP@D2 and showed that the FC curves are always slightly shifted to the negative fields. Table 1 summarizes the coercitive field Hc and exchange field He values for NP@OA and NP@ D2-DE deduced from FC curves. The exchange field of NP@D2-DE is slightly lower than the one of NP@AO. The decrease of He after dendronization highlighted a decrease of the exchange interactions between surface spins and spins of the NPs core. This result showed a reduction of spin canting in canted layer after grafting phosphonate dendron at the surface of iron oxide. This confirmed again the strong anchoring of dendron at the NPs surface through phopshonate groups.

Table 1. Coercitive field, relative remanent magnetization and saturation magnetization for NP before and after functionalization, Coercitive and exchange fields at 5K deduced from FC curves.

Sample	Hc at 5K	Mr/Ms at 5K	Ms at 5K	Ms at 300K	Hc (FC) at 5K 2T (Oe)	He (FC) at 5K 2T (Oe)
NP@AO	377±30	0,26±0.005	50±5	45±5	368±30	-155±30
NP@D2	325±30	0,29±0.005	55±5	46±5	324±30	-108±30

The direct ligand exchange process led to very stable and reproducible suspensions with a mean hydrodynamic diameter below 50 nm. Thus these NPs fulfilled the mandatory conditions for *in vivo* injections. Furthermore, these NPs displayed good magnetic properties, their interactions with cells and in vitro MRI properties were thus also studied.

Cell internalization studies

Several physical characteristics, like size and shape, or chemical surface modifications can influence NPs biodistribution and cell internalization. Depending on the future use of NPs, it could be interesting to control the interaction of NPs and the plasma membrane. It is also of paramount importance to investigate the cell internalization of NPs to decipher if the coating process by itself influences such process. To this aim, Huh7 cells were incubated in the presence of 0.5 mg/mL fluorescently labeled NP@D2 for 24h or 48h. By flow cytometry,

the percentage of cell exhibiting fluorescence, marking NPs internalization, was assessed. As shown in the figure 5, NP@D2-PT are more efficiently internalized than NP@D2-DE with respectively 4 % ± 0.7 and 2 % ± 0.15 at 24h and 22.1 % ± 8.4 and 1.77 % ± 0.4 at 48h of positive cells. Recording of the mean fluorescence gave the same results. Altogether it showed that interaction of NP@D2-DE with plasma membrane is relatively inhibited. However even for NP@D2-PT the number of positive cell is rather low. The experience was repeated and cells observed by fluorescence microscopy instead of flow cytometry after cell nucleus staining with DAPI. One representative picture is shown in an inset of the figure 5. Some cells showed a punctuate green fluorescence. It was a characteristic image of NPs in cell after endocytosis when NPs are gathered in endocytic vesicles. Indeed, regarding the resolution of a fluorescence microscope clusters of NPs are only seen. Moreover it proves that the fluorescence recorded by flow cytometry is not due to the fluorescent dye release from the NPs surface as it would have appeared fainter and homogeneously distributed inside the cell cytoplasm.

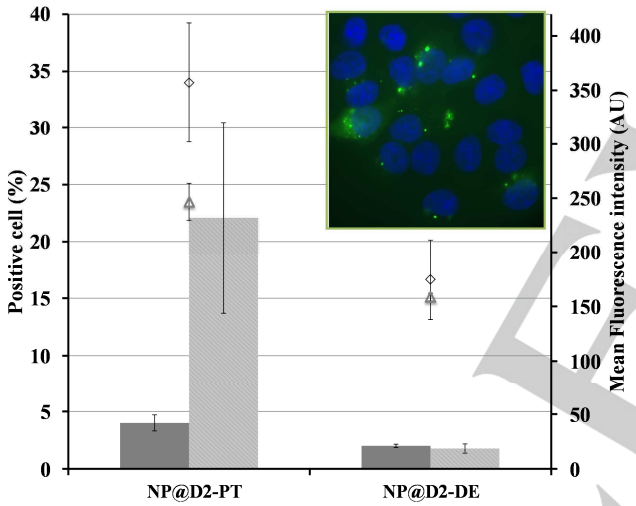

Figure 5 : Internalisation of NP@D2-PT and NP@D2-DE in Huh7 evaluated by flow cytometry. The bars represent the percentage of positive cells at 24h (dark grey) and 48h (dashed). Mean of fluorescence intensity are represented in dots (triangle = 24h; diamond = 48h). Each value represent Mean ± Std error. The inset represent Huh7 cell incubated for 24h with NP@D2-PT fluorescently labeled observed by fluorescence microscopy after nucleus staining with DAPI.

Then, a measurement of the endocytosis of these NPs was carried out in a 3D culture model (Spheroid) of Huh-7 cells. This suspended drop culture method allowed the formation of a cluster of spherical, spheroid-shaped cells that simulate the onset of tumor growth *in vivo* (Figure 6). 3D Huh-7 cell spheroids were incubated 24h with the NPs at a concentration of 0.5 mg/ml. The spheroids were fixed to paraformaldehyde 3.7% and then labeled with PKH26 (red fluorescent marker for general labeling of the membranes). The spheroids were then observed by confocal microscopy. Figure 6 shows a cross section of spheroids incubated with NPs: it confirms that the internalization of the NPs is weak and localized at the periphery of the spheroids. Therefore even if the Huh-7 cells have been noticed to be difficult to transfect, these results suggest a low internalization of dendronized NPs and indicate that the internalization of NP@D2-PT is the result of a non-specific contact and could be related to the NPs'sedimentation on the cells at the bottom of the culture well due to their larger particle size (i.e. aggregation state).

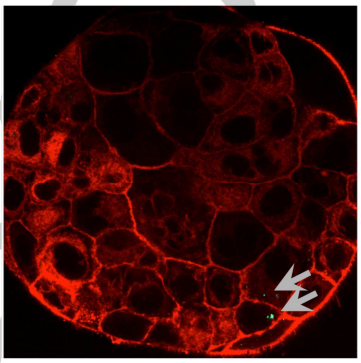

Figure 6 : Confocal laser scan microscopy image (X10 magnification) of Huh-7 spheroid (culture time 4 days) after 24h incubation with 0.5 mg / mL NP@D2-PT.

In vitro and in vivo MRI experiments

Relaxivity measurements were performed for dendronized NPs at 0.47 (20 MHz), 1.41 (60 MHz) and 7 T (300MHz). The longitudinal r_1 and transverse r_2 relaxivities are given in Table 2 and compared to those of commercial products and of 10 nm NPs dendronized with dendron ANACOOH.[39,41] To be used as T_2 contrast agents, the NPs have to display both a high transverse relaxivity r_2 and a high ratio r_2/r_1.[2,3] The values determined at 0.47 and 1.5T (Figure S11) for both dendronized NPs are in agreement with values reported for commercial products or published NPs displaying similar hydrodynamic size. Indeed the agregation state is very important to consider as it contributes to the enhancement of relaxivity values. The difference in relaxivities values and ratios between D2, D2-2P and ANACOOH may be thus mainly related to the different aggregation states (e. g. hydrodynamic size).

Table 2. Relaxivity values for dendronized NPs.

Samples	Coating	d (nm)	D_h (nm)	r_1	r_2	r_2/r_1	B (T)
Ferridex/endorem	Dextran	5	120-180	10.1	120	11.9	1.5
Resovist (Schering)	carboxyd extran	-	60	9.7	189	19.5	1.5
Ferumoxytol (Adv. Magnetics)	Carboxyd extran-dextran T10		30	15	89	5.9	1.5
Supravist (Schering)	Carboxyd extran		21	10.7	38	3.6	1.5
Sinerem (Guerbet)	Dextran		15-30	9.9	65	6,5	1,5
Our samples with $Fe_{3-x}O_4$ NPs	Dendron : ANACOOH	10	30	6.2	91	15	1.5
	Dendron	10	18	27	67	2.5	0.5

synthesized by thermal decompositi on	D2			13	74	5.6	1.5
				2.5	131	52.4	7.0
	Dendron D2-2P	10	16	24	67	2.8	0.5
				11	72	6.5	1.5

The contrast enhancement properties of NP@D2-ED were then evaluated *in vitro* by MRI at 7 T and ghost images (Figure 7) showed a very strong T_2 effect as illustrated by the strong negative T_{2w} contrast. The EHC measurements as a function of the iron concentration given in Figure 7 evidenced a very important T_2 effect even at low iron concentration : EHC T_{2w} = -33.1% at the very low iron concentration of 0.020 mM. A total signal extinction is even noticed at high concentration. The high negative T_{2w} enhancement contrast ratio (EHC) values obtained here for these dendronized NPs, even at high magnetic field (7T) and very low iron concentrations confirmed again the high contrast power of dendronized NPs. Furthermore MR images with iron concentration larger than 1.35 mM are not detected due to their dramatic signal inhibition, preventing their EHC quantification (superior to 100%).

In T1w images, no signal is observed at low concentration but at high concentrations, a hyposignal is noticed: at concentrations of 2.02 and 1.35 mM in iron, the % EHC T_{1w} are -87.6% and -66.9% respectively related to a T2 effect (Figure 7). The strong T2 effect at high concentration can be related to the strong T_2 shortening and also to a NPs clustering favored at such high concentration.[37,63]

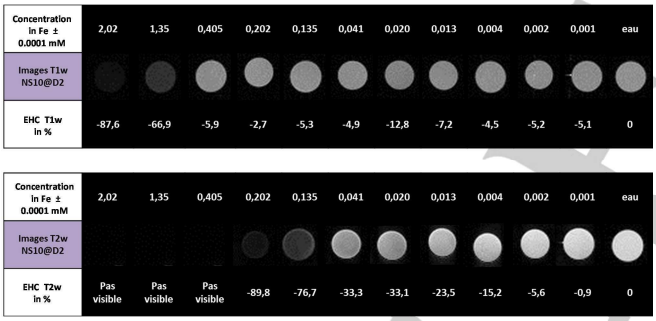

Figure 7 : Ghost images of NP@D2-ED obtained at 7T and 25°C.

From deduced relaxivity values, longitudinal and transversal relaxivities were determined with r_1 = 2.5 $s^{-1}.mM^{-1}$, r_2= 131 $s^{-1}.mM^{-1}$ leading to a ratio r_2/r_1 = 52.4 (Table 2 and Figure S12). The r_2 value at 7T is higher than those reported at 0.47T et 1.5T in agreement with the theory[41] and with earlier results obtained with other dendronized NPs.[25,27]

In vivo MRI images were recorded after intravenous injections of a very moderate quantity of NP@D2-ED (around 5 µg iron/ kg body rat) in rats to confirm the impact of our suspensions NPs on the MRI contrast in the organs. Figure 8 showed MRI images centered on the kidney, aorta, liver and bladder. A signal decrease/ darkening is observed in the spleen, the bladder and the aorta (Figure 8) after injection, confirming again the *in vivo* T2 effect of dendronized NPs even with a small difference in the dendron architecture. These MRI contrast enhancements at short times after iv injection suggested a blood circulation of dendronized NPs and an urinary elimination.

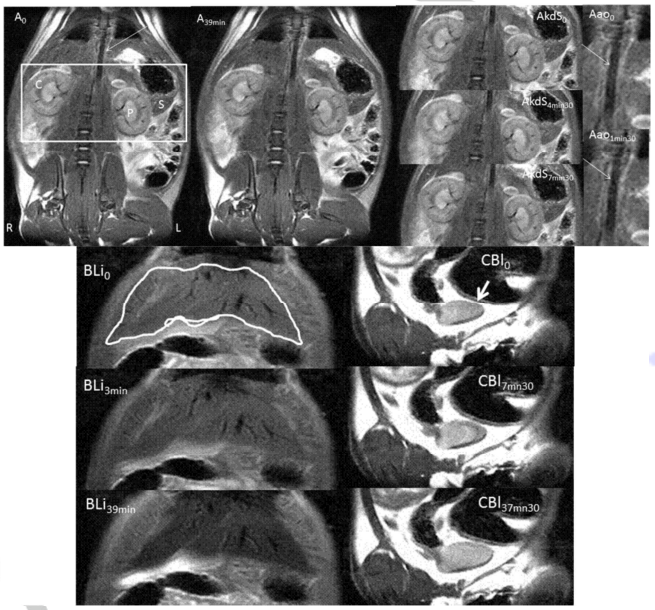

Figure 8 : T_{2w} (rapid echo sequence T_2 ([TR/TE = 800/9.1 ms]; flip angle=180°, 3 mm section thickness, 10x10 cm field of view, 256 x 256 matrix) images centered on aorta (arrow), kidneys (C=cortex, P=pyelon) and spleen (S) before injection (A_0), or bladder (Bl) and liver (Li) before injection (B_0) and 39min IV post-injection. After intravenous injection (catheter in the saphen vein) in a rat under gas anesthesia (A_{39mn}, B_{39mn}). Zoom images on aorta before injection (Aao_0) and 1min30 post injection (EHC = -25%), kidneys and spleen, before injection ($AkdS_0$), 4min30 post injection ($AkdS_{4mn30}$) + 16.5%) and 7min ($AkdS_{7mn30}$) - EHC pyelon G = + 14.5% Zoom T2w images on liver (B- ROI white line) before injection (BLi_0), after 3min (BLi_{3mn30}) corresponding to EHC=+5% and at the end of acquisition (BLi_{39mn}), with maximum EHC= -43%. Zoom T2w images on bladder (arrow) before injection (Bli_0), at maximum EHC signal, at 7min30 (Bli_{7mn30}) – EHC = -5%) and at the end of acquisition (Bli_{37mn30}) –EHC= +2%.

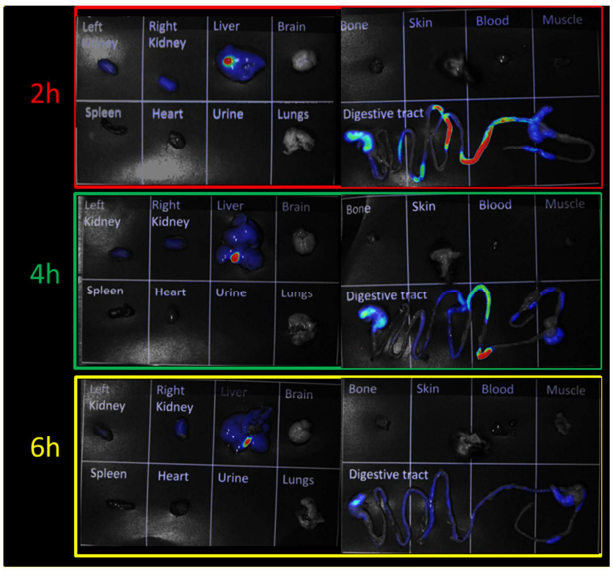

Figure 9 : Qualitative optical imaging analysis : example of normalized optical images of all organs removed in one mouse sacrificed at 2, 4 and 6 h post intravenous (iv) injection of NP@D2-ED.

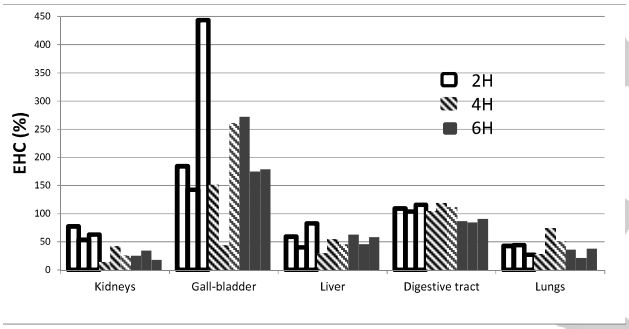

Figure 10 : Semi-quantitative analysis of optical imaging : Values of enhancement of signal (EHC) corresponding to the whole kidneys, liver and gall-bladder measured at 2h, 4h and 6 h after IV of injection of NP@D2-ED in reference to the same organs of not injected mouse.

To further evaluate their bioelimination, NP@D2-ED were coupled to an Alexa dye (Alexa647) via carbodiimidation. As evidenced in figure 9, the qualitative analysis of optical images of organs removed in the 3 mice sacrificed at 2, 4 and 6 h post intravenous (iv) injection of NP@D2-ED allowed to conclude to the absence of large aggregates (not evident lung fluorescent signal), the fast and/or low urinary urinary elimination (low kidney signal and absence of urinary signal at 2h after injection), a fast and high hepato-biliary elimination (high digestive tractus and gall-bladder (behing liver) signal since 2h after IV injection), a slightly lower liver signal at 6h post-IV. Semi-qualitative analysis of optical imaging (Figure 10) confirmed a fast elimination (before 2 hours post-IV) of the NP@D2-ED after IV injection by both urinary and hepato-biliary ways. This analysis confirmed also the very low and not persistent lung uptake. The signal in the liver after 2h does not further increase and even tends to decrease but longer analysis time would have been necessary to conclude unambiguously.

Conclusions

Iron oxide NPs were functionalized with two dendrons molecules bearing one or two phosphonate groups by two methods: the direct exchange of ligand in an organic solvent and the ligand exchange and phase transfer process. The molecules grafting on the surface of the NPs via the phosphonate group has been confirmed by XPS and IR spectroscopy. IR spectroscopy and XRD analysis showed a slight oxidation of NPs following the NPs functionalization. However, the magnetic properties are preserved during this functionalization step: NPS are superparamagnetic and the NPs saturation magnetization is maintained (although oxidation) due to the presence of the surface phosphonate complexes decreasing the surface canted layer contribution.

XPS analysis showed that whatever the dendron, the molecule anchoring is strong, but it is even stronger in the case of the ligand exchange and phase transfer. This is probably due to stronger interactions between molecules and NPs (electrostatic interactions) during this grafting process.

However the ligand exchange and phase transfer method led to suspensions with hydrodynamic diameter larger than 100 nm which rapidly precipitated while the direct exchange process allowed obtaining very stable suspension with a mean hydrodynamic diameter smaller than 50 nm in a simple and reproducible manner.

The nature of the dendron and more particularly the number of anchoring groups present on the dendron molecule did not affect the colloidal stability and hydrodynamic diameter obtained. Only the grafting method determined the hydrodynamic diameter of the suspensions stability. Likewise, the grafting method determined the molecule anchoring strength.

The strong functionalization anchoring, the small hydrodynamic diameter, the strong darkening effect obtained during in vivo MRI experiments and their good bioelimination assessed by optical imaging confirmed the potential of the dendronized NPs to be used as contrast agent for MRI. .

Experimental Section

Synthesis of oleic acid-coated iron oxide nanoparticles

Iron oxide NPs with an average diameter size of 10 nm were synthesized by thermal decomposition of an iron stearate complex in presence of oleic acid in a high boiling point solvent. 1.38 g (2.22 mmol) of $Fe(stearate)_2$ and 1.25 g (4.4 mmol) of oleic acid (OA) were added to 20 mL of octyl ether (b.p 288°C). The mixture was kept at 110°C without stirring during 1h until all the reactants were completely dissolved and the mixture was homogeneous. The solution was then heated at 288°C with a heating rate of 5°C/ without stirring and was refluxed for 120 min at this temperature under air. The resulting black solution was then cooled down to room temperature and the NPs were precipitated by addition of

ethanol and by centrifugation (14 000 tr/min, 10min). The as-synthesized NPs, named NP@OA, were then easily suspended in THF.

Dendron used to functionalized the NPs

We already reported the synthesis of the two dendron molecules.[13,42,43] The scheme of the dendron D2 and D2-2P are presented in the Figure 1.

Nanoparticles functionalization methods

Here, two different functionalization methods were used: a direct grafting process occurring in an organic solvent and a phase transfer grafting process during which the NPs were transferred from an organic solvent to a water phase. The two methods are described below.
For the direct grafting process, a suspension of 1mL of NP@OA in THF (5 mg/mL) was put in contact with 7 mg of Dendron molecule in 4 mL of THF. The mixture was magnetically stirred during 24h. The NP@dendron were then precipitated by addition of hexane and centrifugation (8000tr/min, 3 min). The supernatant was eliminated and the NPs were easily dispersed in 10mL DI water.
For the functionalization through a phase transfer process, 10 mL of NP@OA suspension in hexane (1 mg/mL) were put in contact with a solution of molecule (7 mg molecule, 5 mL water and 2 mL methanol). Both immiscible suspensions were magnetically stirred for one night. A ligand exchange and phase transfer occurred leading to a water suspension of dendronized NPs.
After both grafting processes, the grafted NPs were then separated from the ungrafted dendrons molecules by ultrafiltration. After at least 4 purification steps, the pH of the NPs suspensions was adjusted to 7 and the suspensions were ready for characterizations.

NPs characterization techniques

The NP@OA were characterized by transmission electron microscopy (TEM) with a TOPCON 002B microscope operating at 200 kV (point resolution 0.18 nm). The size distribution of NPs was calculated from the size measurements of more than 300 nanoparticles using ImageJ software.
The NP@OA were also characterized by X-ray diffraction (XRD) using a Bruker D8 Advance equipped with a monochromatic copper radiation source, (Kα = 0.154056 nm) and a Sol-X detector in the 25-65° range with a scan step of 0.03°. High purity silicon powder (a=0.543082 nm) was systematically used as an internal standard. All the diffraction patterns were analysed by the Rietveld method using the Fullprof program for which the modified Thompson-Cox-Hasting pseudo-Voigt profile function was chosen to generate the line shape of the diffraction peaks.

Hysteresis cycle at room temperature and ZFC/FC measurements between 5K and 300K under a field of 75G of the as synthesized NPs were performed with a Superconducting Quantum Interference Device (SQUID).
The ligand exchange at the surface of the NPs was confirmed by infrared spectroscopy using a Fourier Transform Infrared (FTIR) spectrometer and X-ray Photoelectron Spectroscopy (XPS). Infrared spectra were recorded between 4000 and 400 cm^{-1} with a Fourier transform infrared (FTIR) spectrometer, Digilab Excalibur FTS 3000 series. Samples were gently ground and diluted in non absorbent KBr matrixes.
The grafting rate was determined by elemental analysis which has been performed by ICP-MS (Induced Coupled Plasma Mas Spectrometry). The stability of the grafted NPs was assessed using a nano-size MALVERN zetasizer.

The NP@OA were characterized by X-ray diffraction (XRD) using a Bruker D8 Advance equipped with a monochromatic copper radiation source, (Kα = 0.154056 nm) and a Sol-X detector in the 25-65° range with a scan step of 0.03°. High purity silicon powder (a=0.543082 nm) was systematically used as an internal standard. All the diffraction patterns were analysed by the Rietveld method using the Fullprof program [44] for which the modified Thompson-Cox-Hasting pseudo-Voigt profile function was chosen to generate the line shape of the diffraction peaks. [45]
XPS analyses were conducted with a Kratos Axis Ultra DLD spectrometer (Kratos Analytical Ltd, Manchester, UK) using focused monochromatized Al Kα radiation (hv = 1486.6 eV). The samples were transferred in the XPS spectrometer with a transfer vessel. To prevent any moisture or air exposure of the samples, the XPS spectrometer was directly connected to an argon dry box working at low H_2O/O_2 levels (<10 ppm through a fast load transfer chamber). The analysis chamber conditions were held constant under ultra-high vacuum (pressure < 2.10^{-7} Pa). The spectrometer was fitted with a double focusing 180° hemispherical analyzer (HSA) and a spherical mirror analyzer (SMA), which were run in fixed analyzer transmission mode (FAT) for the XPS data acquisition (FAT also known as constant analyzer energy mode, CAE). The detector system was based on delay-line detection used for both spectroscopy and 2-D imaging applications. The instrument work function was calibrated to produce a binding energy (BE) of 83.96 eV for the Au $4f_{7/2}$ line for metallic gold and a BE of 932.67 eV for the Cu $2p_{3/2}$ line for metal copper. The performance of the spectrometer on the Ag 3d 5/2 photoemission line (BE 368.3 eV) was 250 000 counts at 0.48 eV full width at half maximum normalized to the full X-ray power. The coaxial Kratos patented charge neutralizer was used during the analysis to avoid any charge effect (i.e., coaxial electron flood gun working in accordance with a magnetic immersion lens). Survey spectra (wide energy range from -5.0 eV to 1200.0 eV BE) were recorded at a constant pass energy (PE) of 160 eV (CAE mode) in high magnification lens mode for high sensitivity conditions at a power of 100 watts (10 mA/10 kV). Core ionization peaks were recorded at a constant PE of 20 eV. The spectral calibration was done by rescaling the experimental profiles based on the hydrocarbon contamination component of the C 1s peak (285.0 eV). The peak fitting was processed with a nonlinear Shirley-type background and the mathematical components were optimized by a weighted least-squares fitting method using 70% Gaussian and 30% Lorentzian line shapes. The quantification was performed with the CasaXPS processing software (CasaXPS Ltd, Teignmouth, UK) using Kratos relative sensitivity factors.
For functionalized NPs, the temperature in the analysis chamber was kept at 25°C, but for the dendron D2 and D2-2P, it was regulated at -160°C to avoid the possible degradation due to X-ray beam and possible sublimation of the compound under vacuum.

Cell studies

Cell : Human hepatocarcinoma Huh7.5.1 cells were propagated in Dulbecco's modified Eagle's medium supplemented with 10% of decomplemented foetal bovine serum, gentamycine (50µg/mL) and non-essential amino acids.
Flow cytometry: Huh7 (2. 105 cells per well) were seeded in a 24-well plate (Greiner, Dominique Dutscher, ref 165305) and kept overnight for attachment. Cell were then incubated, with 1 mL per well of NP diluted in complete medium, for 24 or 48h at 37°C in 5% CO2. Cells were then thoroughly rinsed with 1 mL of cold PBS. Cells were then incubated with 300 µL of tryspin/EDTA solution (GIBCO, Ref R001100, Thermofisher) for 5 minutes. Cells were then resuspended by addition of 500 µL of PBS and harvested by centrifugation at 1000 rpm for 5 min. Cell were resuspended in 1 mL PB + 2% paraformaldehyde (PFA) and kept at 4°C protected from light until analysis. Cell fluorescence was analyzed by

flow cytometry using a FACScan flow cytometer with Novios software. Cells were analyzed in FL1 canal (Exc 488 nm Em 505 nm). Fluorescence threshold was determined using none treated cells. 10 000 cells were analyzed by sample. Results are reported as the percentage of cell presenting fluorescence above the aforementioned fluorescence threshold.
Fluorescence microscopy: 24h prior the experiment, Huh-7 cells were seeded in Lab-Tek® 8 chamber slide at a concentration of 1.10^5 cell per well. Then the cells were incubated with complete medium with NP@D2-ED and NP@D2-PT for 24h. The cells were subsequently fixed with paraformaldehyde 3.7% in PBS. The lamellae were mounted for observation by fluorescence microscopy with a medium containing DAPI (4,6-diamidino-2-phenylindole, fluorescent dye used in fluorescence microscopy which becomes highly fluorescent when interacting with DNA.) in order to highlight the nuclei. fluorescence images were captured using Nikon Elipse TE200 with 63× PL APO (1.4 NA) objectif equipped with Nikon Digital Camera (DS-Q11MC with NIS-Elements softwares), and processed with ImageJ (http://rsb.info.nih.gov/ij/).

Preparation of Huh-7 tumor spheroid: Prior to the culture, sterile 96-well plates equipped with a lid (Corning™ Costar™ Flat Bottom Cell Culture Plates, Fisher scientific, Ref 10792552) were coated with poly(2-hydroxyethyl methacrylate) (poly-HEMA; sigma P3932-10G). The coating was done by addition of a 0.5 % (w/v) poly-HEMA solution in ethanol (100 µL) into each well of a 96-well plate at 38°C. The plate was kept at 38°C for 24h for complete ethanol evaporation and for ensuring surface coating. PBS (100 µL) was then added into each well. Adherent Huh-7 were treated with trypsin and suspended in complete medium at 5.3 10^3 cell/mL. The cell suspension (15 µL) were deposited on the inside face of the 96-well plate lid. The lid was then replaced on the PBS-filled plate and the cells in the hanging drop were led to grow in the incubator for 3 days. The PBS was then discarded and replaced with complete cell culture medium (100 µL). Each drop containing one single spheroid was then transferred from the lid into the well by centrifugation at 500 RPM for 1 minute.
Evaluation of particle diffusion in Huh-7 spheroids: The experiments were carried in triplicate. Huh-7 spheroid was incubated in a complete cell culture medium for 24 h with Rho-SiC/□PEI polyplexes N/P 14 at final concentrations of 180 µM siRNA and 100 µM πPEI. The spheroids were then fixed by addition of 8% (w/v) paraformaldehyde (EMS group, Hatfield, PA, USA) in PBS (100 µL) to each well. After 15 min, fixed Huh7 spheroids were harvested with a 400 □m fiber loop and incubated for 5 min in PBS (100 µL). The cell membranes were then stained using the red fluorescent PKH26 staining kit (Sigma Aldrich, St Quentin, France) following manufacturer instruction. After membrane staining, the tumors were rinsed in PBS and were mounted in an Antifade Mounting Medium (Vector laboratories, H-1000, Burlingame, CA). For imaging, excitation wavelengths were set at 488 nm and 543 nm for triggering NPs and membrane stain fluorescence, respectively. Green and red light emissions were recorded after filtration using 505-530 nm band-pass and 585 nm long pass filters. Several images were recorded along the z-axis for focal sectioning.

MRI experiments

MRI contrast effects of the dendronized NPs were evaluated firstly in vitro at 7T using a small animal dedicated 7T MR Biospec™ system (Brüker, Wissenbourg, France) equipped with 400 mT/m gradient by imaging 900 microliter water samples containing increasing iron concentration (from 0 to) with an inversion recovery FLASH (IR-FLASH) imaging sequence with varying IR, allowing to calculate the spin-lattice (R1) and spin-spin (R2) relaxivities defined as the concentration-independent measures of the relaxation rate enhancement for respectively the longitudinal and transverse magnetization components..

Then, a common T1weighted (spin-echo sequence -TR/TE = 500/12 msec) and T2 weighted sequence (multi- spin echo sequence - TR/TE = 2000/70 msec] imaging sequences were acquired in order to assess the T1 or T2 effect in function to the iron concentration, by calculating the value of the enhancement (EHC) [EHC (%)w= [(((Signal value of dendronized NPs) – (signal value of water))/signal value of water)x 100].of the contrast in comparison to the water sample (a positive value of the EHC indicated a T1 effect at contrary of a negative EHC value, indicating a T2 effect).

In order to assess as *in vivo* MRI contrast agent and evaluate its biokinetics, we analyzed the in rats under gaseous anesthesia (Isoflurane®, Laboratoire Belamont, Neuilly-sur-Seine, France) using an experiment protocol approved by the local animal ethic committee. To improve the quality of the vascular distribution after intra-venous injection the compounds were injected via a catheter inserted inside the saphen vein just before the MRI acquisition, and in order to decrease breathing moving artefacts, each acquisition was triggered on respiration (Rapid Biomedical GmbH). T1 and T2 MR contrast effects were assessed using two different type of sequences: i) a multi- gradient echo sequence (repetition time (TR) = 800msec, 12 echos- echo spacing = 2.56 msec – 1st echo time (TE) = 1.54 msec, 2 mm section thickness, 10x7 cm field of view, 256x128 matrix); ii) a rapid echo sequence T_2 ([TR/TE = 800/9.1 msec]; flip angle=180°, 3 mm section thickness, 10x10 cm field of view, 256 x 256 matrix, for respectivitly T1 and T2 effect studies. About 90 sec (for T1W sequence) and 2-3 mn (for T2w) series of coronal slice centered on kidneys (cortex and pelvic cavity), liver and bladder were acquired before and over 1h after injection of around 2 µM/kg of iron.

The mean value signal (S) was measured at each time point in Region Of Interest (ROI) corresponding to liver, kidneys (whole organ and/or renal cortex, and urinary intra-renal excretion cavities called “pyelon”), bladder and if visible, to the aorta. In order to quantify the in vivo MR contrast effect of dendronized NP in function of iron mass injected, post-injection delay, the contrast enhancement (EHC) related to the focal dendronized particles deposition was calculated in each ROIs as defined: EHC = [SN(t) – SN(bi)/ SN (bi)].

Fluorescence Imaging

To determine the delay of the bioelimination of the dendronized NP, NP@D2-ED were coupled to an Alexa dye (Alexa647) via carbodiimidation.One hundred µl of dendronized NP solution were intra-venously injected in 9 nude mices under gaseous anesthesia (Isoflurane®, Laboratoire Belamont, Neuilly-sur-Seine, France). Three mice were sacrificed at 2h, 4 h and 6 h after IV injection and main organs (spleen, lungs, liver, kidneys, brain, heart, digestive tract, and a sample of bone, skin, muscle and eventually, of urine) were removed and imaged with a back thinned CCD-cooled camera (ORCAIIBT-512G, Hamamatsuphonics, Massy, France) using a colored glass long-pass RG 665filter (Melles Griot, Voisins les Bretonneaux, France). Qualitative (visual analysis) and semi-quantitative analysis was performed by calculating the signal enhancement in main organs related to the Dye grafted on NPs, by comparison with signal in same organ removed from mice not injected and imaged with the same parameters(S_0) [EHC (%) = ((S - S_0) /S_0)x100]. Elimination pathways and kinetic assessing was based on qualitative (significant fluorescent signal in urine, in gall-bladder and digestive tract for hepato-biliary elimination) and kinetic parameters based on time evolution of EHC in mains organs.

Acknowledgements

We thank the CNRS, University of Strabourg and the French Ministry of Research (fellowship to A. Walter) for financial support. This work was also supported by the program «Nano@matrix» INTERREG IV Upper Rhine Valley. «Transcending borders with every project » (fellowships to A. Garofalo), by the Institut Carnot MICA and by ARC foundation (THERA HCC project). We also thank Celine Kiefer (chemicals management), Corinne Ulhacq (TEM), Emilie Voirin and Emilie Couzigné (technical assistance).

Keywords: iron oxide nanoparticles • dendron coating • functionnalization process • size distribution • in vitro and in vivo MRI

[1] M. Liong, J. Lu, M. Kovochich et al. *ACS Nano,* **2008**, *2,* 889-896; J. Kim, Y. Piao, T. Hyeon, *Chem. Soc. Rev.,* **2009**, *38,* 372-390; M. De, P.S. Ghosh, V.M. Rotello, *Adv. Mater.,* **2008**, *20,* 4225-4241; S. Mornet, S. Vasseur, F. Grasset, E. Duguet *J. Mater. Chem.,* **2004**, *14,* 2161-2175; D. Yoo, J-H Lee, T-H Shin, J. Cheon, Acc. Chem. Res., **2011**, *44*, 863-874;

[2] C. Blanco-Andujar, A. Walter, G. Cotin, C. Bordeianu, D. Mertz, D. Felder-Flesch, S. Bégin-Colin, *Nanomedicine (Future Medicine)* **2016**, *11*, 1889-1910.

[3] S. Laurent, D. Forge, M. Port, A. Roch, C. Robic, L. Vander Elst, R. N. Muller, *Chem. Rev.,* **2008**, *108,* 2064-2110.

[4] A.K. Gupta, M. Gupta,. *Biomaterials*, **2005**. *26*, 3995-4021.

[5] A. Figuerola, R. D. Corato, L. Manna, T. Pellegrino, *Pharm. Res.,* **2010**, *62*, 126-143.

[6] S. Mornet, S. Vasseur, F. Grasset, E. Duguet, *J. Mater. Chem.*, **2004**, *14*, 2161-2175.

[7] M. Colombo, S. Carregal-Romero, M.F. Casula, L. Gutiérrez, M.P. Morales, I.B. Böhm, J.T. Heverhagen, D. Prosperi, W.J. Parak, *Chem. Soc. Rev.,* **2012**, *41*, 4306-34.

[8] A.-H. Lu, E.L. Salabas, F. Schath, *Angew. Chem. Int. Ed. Engl.,* **2007**, *46*, 1222-44.

[9] A. Walter, A. Parat, A. Garofalo, S. Laurent, L. Vander Elst, R. N. Muller, T. Wu , E.Heuillard, E. Robinet, F. Meyer, D. Felder-Flesch, S. Begin-Colin, *Part. Part. Syst. Charact.,* **2015**, *32*, 552–560.

[10] A. Walter, A. Garofalo, A. Parat, H. Martinez, D. Felder-Flesch, S. Begin-Colin, *Nanotechnology reviews*, **2015**, *4*, 581-593

[11] A. Parat, C.Bordeianu, H. Dib, A. Garofalo, A. Walter, S. Bégin-Colin, D. Felder-Flesch, *Nanomedicine*, **2015**, *10*, 977-992.

[12] A. Walter, A. Garofalo, P. Bonazza, A. Parat, J. Taleb, J. Jouhannaud, G. Pourroy, E. Voirin, S. Laurent, L. Vander Elst, R. N. Muller, C. Billotey, S. Begin-Colin, D. Felder-Flesch, *J. Mater. Chem. B*, **2015**, *3*, 1484-1494.

[13] A. Garofalo, A. Parat, C. Bordeianu, C. Ghobril, M. Kueny-Stotz, A. Walter, J. Jouhannaud, S.Begin-Colin, D. Felder-Flesch, *New J. Chem.*, **2014**, *38*, 5226-5239.

[14] Dendrimers in Nanomedicine, Edited by Delphine Felder-Flesch, Penthouse Level, Suntec Tower 3, 8 Temasek Boulevard, Singapore 038988 Pan Stanford Publishing Pte. Ltd. 2016.

[15] N. Fauconnier, J.N. Pons, J. Roger, A. Bee, *J. Colloid Interface Sci.*, **1997**, *194,* 427-433.

[16] M. Lattuada, T.A. Hatton, Langmuir, **2006**, *23*, 2158-68.

[17] L. Maurizi, H. Bisht, F. Bouyer, N. Millot, Langmuir, **2009**, *25*, 8857-8859.

[18] N. Miguel-Sancho, O. Bomatí-Miguel, Gloria Colom, J-Pablo Salvador, M-Pilar Marco, J. Santamaria, *Chem. Mater.,* **2011**, *23*, 2795-2802.

[19] M. Răcuciu, D.E. Creangă, A. Airinei, *Eur. Phys.J. E*, **2006**, *21*, 117-121.

[20] E. Amstad, S. Zurcher, A. Mashaghi, J.Y. Wong, M. Textor, E. Reimhult, *Small*, **2009**, *5*, 1334-1342.

[21] N.A. Frey, S. Peng, K. Cheng, S. Sun, *Chem. Soc. Rev.,* **2009**, *38*, 2532-2542.

[22] T. J. Daou, J.M. Grenèche, G. Pourroy, S. Buathong, A. Derory, C. Ulhaq-Bouillet, B. Donnio, D. Guillon and S. Begin-Colin, *Chem. Mater.,* **2008**, *20*, 5869-75.

[23] T. J. Daou, S. Buathong, D. Ung, B. Donnio, G. Pourroy, D. Guillon, S. Bégin, *Sensor and actuator B*, **2007**, *126*, 159-162.

[24] B. Basly, D. Felder-Flesch, P. Perriat, G. Pourroy, S. Bégin-Colin, *Contrast Media & Molecular Imaging,* **2011**, *6*, 132–138.

[25] B. Basly, D. Felder-Flesch, P. Perriat, C. Billotey, J. Taleb, G. Pourroy, S. Begin-Colin, *Chem. Comm.,* **2010**, *46*, 985-987.

[26] E. D. Smolensky, Hee Yun E Park, T. S. Berquó, V. C. Pierre, *Contrast Media & Molecular Imaging*, **2011**, *6*, 189-199.

[27] B. Basly, G. Popa, S. Fleutot, B. Pichon, A. Garofalo, C. Ghobril, C. Billotey, A. Berniard, P. Bonazza, H. Martinez, D. Felder-Flesch, S. Begin-Colin, *Dalton Transaction*, **2013**, *42*, 2146-2157.

[28] S. Begin-Colin and Delphine Felder-Flesch, Magnetic Nanoparticles: From Fabrication to Biomedical and Clinical Applications, Editeur Thanh Nguyen, Taylor&Francis, **2011**, 151-191

[29] Y. Sahoo, H. Pizem, T. Fried, D. Golodnitsky, L. Burstein, C. N. Sukenik, G. Markovich, Langmuir, **2001**, *17*, 7907-7911.

[30] Y. Lalatonne, F. Benyettou, D. Bonnin, N. Lièvre, P. Monod, M. Lecouvey, P. Weinmann, L. Motte, J. Magn. Magn. Mater., **2009**, *321*, 1653-1657.

[31] Y. Lalatonne, C. Paris, J.M. Serfaty, P. Weinmann, M. Lecouvey, L. Motte *Chem.Commun.,* **2008**, *22*, 2553–2555

[32] T. J. Daou, S. Bégin-Colin, J.M. Grenèche, F. Thomas, A. Derory, P. Bernhardt, P. Legaré, G. Pourroy, *Chem. Mater.*, **2007**, 19, 4494-4505.

[33] G. Lamanna, M. Kueny-Stotz, H. Mamlouk-Chaouachi, B. Basly, C. Ghobril, C. Billotey, A. Berniard, G. Pourroy, S. Begin-Colin, D. Felder-Flesch, *Biomaterials*, **2011**, *32*, 8562-8573.

[34] C. Bordeianu, A. Parat, C. Affolter-Zbaraszczuk, R. N. Muller, S. Boutry, S Begin-Colin, F.Meyer, S. Laurent, D. Felder-Flesch, submitted to Chemistry of Materials

[35] W. Baaziz, B. Pichon, S. Fleutot, Yu Liu, C. Lefevre, J.-M. Greneche, M. Toumi, T. Mhiri, S. Begin-Colin, *J. Phys. Chem C*, **2014**, *118*, 3795–3810.

[36] M. Pauly, B. P. Pichon, S. Fleutot, P. Panissod, M. Drillon and S. Begin-Colin, *J. Mater. Chem.*, **2012**, *22*, 6343-6350.

[37] M. Pauly, B. P. Pichon, P.-A. Albouy, S. Fleutot, C. Leuvrey, M. Trassin, J.-L. Gallani, S. Begin-Colin, *J. Mater. Chem.*, **2011**, *21*, 16018-16027.

[38] M.G. Nooney, T.S Murrell, J.S. Corneille, E.I. Rusert, L.R. Rossner, D.W. Goodman, *J. Vac. Sci. Technol. A.*, **1996**, *14*, 1357-1361.

[39] C. Ghobril, G. Popa, A. Parat, C. Billotey, J. Taleb, P. Bonazza, S. Begin-Colin and D. Felder-Flesch, *Chem. Comm.*, **2013**, *49*, 9158-9160.

[40] G. Guerrero, P.H. Mutin, A. Vioux, *Chem. Mater.*, **2001**, *13*, 4367-4373.

[41] A. Roch, Y. Gossuin, R.N. Muller, P. Gillis, J. Magn. Magn. Mater., **2005**, *293*,532-539.

[42] P. Chevalier, A. Walter A. Garofalo, I. Veksler, J. Lagueux, S. Bégin-Colin D. Felder-Flesch and M.-A. Fortin, *J. Mater. Chem. B*, **2014**, *2*, 1779-1790

[43] A. Walter, C. Billotey, A. Garofalo, C. Ulhaq-Bouillet, C. Lefèvre, J. Taleb, S. Laurent, L. Vander Elst, R. N. Muller, L. Lartigue, F. Gazeau, D. Felder-Flesch and S. Begin-Colin, *Chem. Mater.*, **2014**, *26*, 5252-5264

[44] J. Rodriguez –Carvajal, *J. Phys. B*, **1993**, *192*, 55-69.

[45] P.Thompson, D. E. Cox., J. B. Hastings, *J. Appl. Crystallogr.,* **1987**, *20*, 79–83.

10.1002/cplu.201700049

WILEY-VCH

Entry for the Table of Contents (Please choose one layout)

Layout 1: Effect of the functionalization process on colloidal, MRI and bioelimination properties of mono or bisphosphonate-anchored dendronized iron oxide nanoparticles

FULL PAPER

The effect of the number of anchoring agent and of the grafting process on the anchoring strength and colloidal, magnetic properties, cell internalization, bioelimination and *in vitro* and *in vivo* MRI properties of dendronized iron oxide nanoparticles

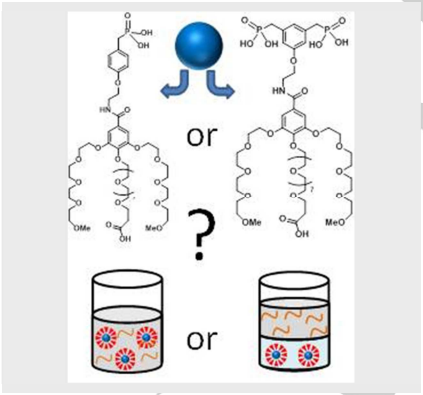

*Author(s), Corresponding Author(s)**

Page No. – Page No.

Title